Target-oriented wavefield tomography: A field data example

Yaxun Tang and Biondo Biondi

ABSTRACT

We present a strategy for efficient migration velocity analysis in complex geological settings. The proposed strategy contains two main steps: simulating a new data set using an initial unfocused image and performing wavefield-based tomography using this data. We show that the new data set can be synthesized for a specific target region where velocities are inaccurate. We also show that the new data set can be much smaller than the original one due to the target-oriented modeling strategy, but it contains necessary velocity information for successful velocity analysis. These interesting features make this new data set suitable for target-oriented, fast and interactive velocity modeling building. We demonstrate the performance of our method on a selected 2-D line of a 3-D data set acquired from the Gulf of Mexico, where we update the subsalt velocity in a target-oriented fashion and obtain a subsalt image with improved continuities and signal to noise ratio.

INTRODUCTION

Velocity estimation is always a challenging task in exploration seismology. In the past decade, ray-based tomography has been widely used in practice to derive velocity models. Although ray-based methods are efficient, the infinite-frequency approximation and the caustics inherent in ray theory prevent them from accurately modeling complicated wave phenomena (Hoffmann, 2001). As seismic exploration is moving towards structurally complex areas, ray-based methods become less reliable. On the other hand, wave-equation-based tomography (Tarantola, 1984; Mora, 1989; Woodward, 1992; Pratt, 1999; Sava, 2004; Shen, 2004) uses wavefields as carriers of information. It more accurately describes the bandlimited wave phenomena, and therefore more suitable for complex geologies.

Wavefield tomography can be implemented in either data domain or image domain. In this paper, however, we mainly focus on the image-domain wavefield tomography, which is also widely known as wave-equation migration velocity analysis (Sava, 2004; Shen, 2004). It derives an optimum velocity model by driving an objective function defined in the image domain to its minimum (or maximum). Despite its advantages in modeling bandlimited wavefields, practical application of image-domain wavefield tomography is still rare and small in scale due to its huge computational

cost (Biondi and Sava, 1999; Shen et al., 2005; Albertin et al., 2006). The high cost arises because of the use of more expensive wavefield modeling engines. The other reason is that it lacks flexibility and the recorded whole data set is usually used for velocity estimation.

Several methods have been proposed to make wavefield tomography more cost effective. The main idea is to reduce the size of the data used for velocity estimation. One method is to assemble the originally recorded point-source gathers into a smaller number of areal-source gathers. But this strategy lacks flexibility, and full-domain wavefield propagation is still required at each velocity inversion iteration. Therefore, the cost reduction can not be substantial.

Biondi (2006, 2007); Guerra et al. (2009); Guerra and Biondi (2010) approach this problem in a completely different way. They synthesize a new data set based on the initial image using the concept of prestack-exploding-reflector modeling. The new data set is then used specifically for velocity analysis. The advantage of this strategy is that it can model a new data set in a target-oriented fashion, therefore the wavefield propagation can be restricted to regions with velocity inaccuracies, substantially reducing the computational cost. However, the modeling generates crosstalk when multiple image events are modeled simultaneously. This limits the number of reflectors to be modeled. Manual picking and stochastic encoding methods, such as random-phase encoding, are required to minimize the impact of the crosstalk (Guerra et al., 2009).

Another way to synthesize a target-oriented data set is through Born wavefield modeling, or demigration (Tang and Biondi, 2010). This technique has been used by Wang et al. (2005), who generate a post-stack data set and use it for efficient subsalt velocity scan. In our method (Tang and Biondi, 2010), however, we generate a prestack Born data set and use it for wavefield-based tomography. As shown by Tang and Biondi (2010), our modeling strategy is very flexible. Except for windowing out the target image from the initial image, no picking is necessary, but picking can also be introduced if it is desired. Human intervention can also be incorporated by carefully conditioning the initial image to be modeled.

Born wavefield modeling is based on the single-scattering approximation to the full wave equation. The modeled data is obtained by convolving the incident source wavefield, computed using any type of source function (e.g. plane-wave sources), with the initial image and then propagating the convolved wavefields to receiver locations, which can be located anywhere in the model. The target-oriented data set is obtained by only modeling image points within a target zone or several key reflectors that carry important velocity information. This target-oriented velocity analysis strategy is useful, because it allows us to use the most powerful velocity estimation tool to focus on improving velocities in the most challenging areas, e.g., subsalt regions, provided that velocities at other locations are sufficiently accurate, e.g., regions above the salt, where the velocities are usually very accurately determined even by ray-based tomography thanks to the relatively simple geologies.

In the next section, we briefly review the theory of Born modeling. In the subsequent sections, we apply the proposed target-oriented velocity-estimation strategy to a field data set acquired from the Gulf of Mexico.

THEORY

Our method can be formulated under the framework of seismic data mapping (SDM) (Hubral et al., 1996; Bleistein and Jaramillo, 2000), where the idea is to transform the original observed seismic data from one acquisition configuration to another with a designed mapping operator. SDM can be summarized into two main steps as illustrated in Figure 1: (1) apply the (pseudo) inverse of the designed mapping operator to the original data set to generate a model; (2) apply the forward mapping operator to the model to generate a new data set with different acquisition configuration than the original one. This idea has been widely used in the area of seismic data interpolation and regularization. For example, in Radon-based interpolation methods (Sacchi and Ulrych, 1995; Trad et al., 2002), Radon operator is used as the mapping operator to regularize the data; the azimuth moveout (AMO) (Biondi et al., 1998) uses dip moveout (DMO) as the mapping operator to transform the data from one azimuth to another.

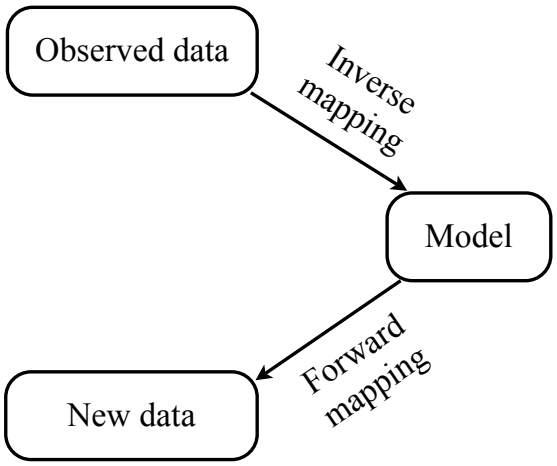

Figure 1: Flow diagrams of seismic data mapping. [**NR**]

In our method, we use wave-equation-based Born modeling or demigration as the mapping operator to peform data mapping. With an initial velocity model, seismic prestack images can be obtained using the pseudo inverse of the Born modeling operator as follows:

$$\mathbf{m} = \mathbf{H}_0^{\dagger}\mathbf{L}_0^{*}\mathbf{d}_{\text{obs}}, \tag{1}$$

where * and † denote adjoint and pseudo inverse, respectively; $\mathbf{m}$ is the seismic image; $\mathbf{L}_0$ is the Born modeling operator computed using initial velocity $\mathbf{v}_0$, whose adjoint $\mathbf{L}_0^*$ is the well-known depth migration operator; $\mathbf{H}_0$ is the Hessian operator (Plessix and Mulder, 2004; Valenciano, 2008; Tang, 2009); $\mathbf{d}_{\text{obs}}$ is the observed surface data.

It is important to note that the seismic image $\mathbf{m}$ has to be parameterized as a function of both spatial location and some prestack parameter, such as the subsurface offset, reflection angle, etc., in order to preserve the velocity information for later velocity analysis (Tang and Biondi, 2010). In this paper, we use the subsurface offset as our prestack parameter. The significance of the Hessian operator in equation 1 is that its pseudo inverse removes the influence of the original acquisition geometry in the least-squares sense and the resulting image is independent from the original data. However, the full Hessian $\mathbf{H}_0$ is impossible to obtain in practice due to its size and computational cost, we therefore approximate it by a diagonal matrix as follows:

$$\mathbf{H}_0 \approx \text{diag}\{\mathbf{H}_0\}. \tag{2}$$

Substituting equation 2 into equation 1 yields

$$\mathbf{m} = \text{diag}\{\mathbf{H}_0\}^{-1}\mathbf{L}_0^*\mathbf{d}_{\text{obs}}. \tag{3}$$

Equation 3 is also widely known as normalized or amplitude-preserving migration (Plessix and Mulder, 2004; Rickett, 2003; Tang, 2009).

We obtain a target image $\mathbf{m}_{\text{target}}$ by applying a selecting operator $\mathbf{S}$ to the initial image as follows:

$$\mathbf{m}_{\text{target}} = \mathbf{S}\mathbf{m}, \tag{4}$$

where the selecting operator $\mathbf{S}$ can be simply a windowing operator. A new data set $\widetilde{\mathbf{d}}_{\text{obs}}$ can then be simulated as follows:

$$\widetilde{\mathbf{d}}_{\text{obs}} = \widetilde{\mathbf{L}}_0\mathbf{m}_{\text{target}}, \tag{5}$$

where $\widetilde{\mathbf{L}}_0$ is the Born modeling operator computed using the same initial velocity $\mathbf{v}_0$, but with different acquisition configuration. The wavefield propagation can be restricted to regions with inaccurate velocities, and the modeled data can be collected at the top of the target region. The target-oriented modeling strategy makes the new data set much smaller than the original one. The new data set can be imaged using the migration operator, i.e., the adjoint of $\widetilde{\mathbf{L}}$, as follows:

$$\widetilde{\mathbf{m}} = \widetilde{\mathbf{L}}^*\widetilde{\mathbf{d}}_{\text{obs}}. \tag{6}$$

We pose our velocity analysis problem as an optimization problem defined in the image domain, where the objective function to minimize is defined as follows:

$$J = ||\mathbf{D}\widetilde{\mathbf{m}}||^2, \tag{7}$$

where $\mathbf{D}$ is the subsurface-offset-domain differential semblance operator (DSO) (Shen, 2004; Shen and Symes, 2008), which is simply a multiplication of the subsurface offset. DSO optimizes the velocity model by penalizing energy at non-zero subsurface offset, utilizing the fact that subsurface-offset gathers should focus at zero subsurface offset if migrated using an accurate velocity model. We evaluate the gradient of equation 7 using the adjoint-state method (Shen and Symes, 2008; Sava and Vlad, 2008; Tang et al., 2008), and use gradient-based methods to optimize the velocity model.

FIELD-DATA EXAMPLES

We test our method on a field data set acquired from the Gulf of Mexico. The data were collected using a narrow azimuth towed streamer (NATS) acquisition system, and further rotated using AMO (Biondi et al., 1998) into zero azimuth. We extracted one crossline from the 3-D data set and performed a 2-D target-oriented wavefield tomography to estimate the subsalt velocity. The extracted data contains 801 shots with the minimum and maximum inline offset equal to 984 ft and 30839 ft. The frequency content ranges from 5 Hz to 35 Hz.

Figure 2 shows the initial velocity model for the extracted 2-D line. Velocities above the target (outlined by a black box) and the salt interpretation are assumed to be accurate. The goal is to invert for subsalt velocities inside the target region. The initial velocities inside the box are set to be $v(z)$. The initial image and subsurface-offset-domain common-image gathers (SODCIGs) obtained using the original data and the initial velocity model is shown in Figure 3. The amplitudes of the initial image have been balanced by the diagonal of the Hessian (Figure 4) according to equation 3 to compensate for uneven subsalt illumination and remove the influence of the original data acquisition geometry. Note the unfocused SODCIGs due to velocity errors.

Then we use the target image (Figure 3) and the Born modeling described in the previous section to generate 31 plane-wave-source gathers at the top of the target region, where the take-off angle is from -30° to 30°. The same starting velocity model that was used for migration (Figure 2) has been used for modeling, and the new data set is collected just above the target region. We only model Born wavefields up to 25 Hz. Figure 5 shows the image migrated using the new data set and the initial velocity (Figure 2). Note the same kinematics shown in Figures 3 and 5. This suggests that the velocity information has been successfully preserved using the new data set, which is substantially smaller compared to the original one.

We minimize the objective function J (equation 7) using a nonlinear conjugate gradient solver. Figure 6 shows the inverted velocity model after 30 iterations. We then migrate the original data set using the inverted model and compare the result with that obtained using the initial velocity model. Figures 7, 8 and 9 compare the stacked section (zero-subsurface-offset image) using the initial and updated velocities. The image obtained using the inverted velocity model shows improved continuities, better focusing and higher signal to noise ratio. The angle domain common image gathers (ADCIGs) migrated using the inverted velocity mode (Figure 10(b)) are also flatter comparing to those obtained using the initial velocity model (Figure 10(a)).

CONCLUSIONS

We have presented a cost-effective method for image-domain wavefield tomography. Instead of using the original data set for velocity estimation, our method uses dem-

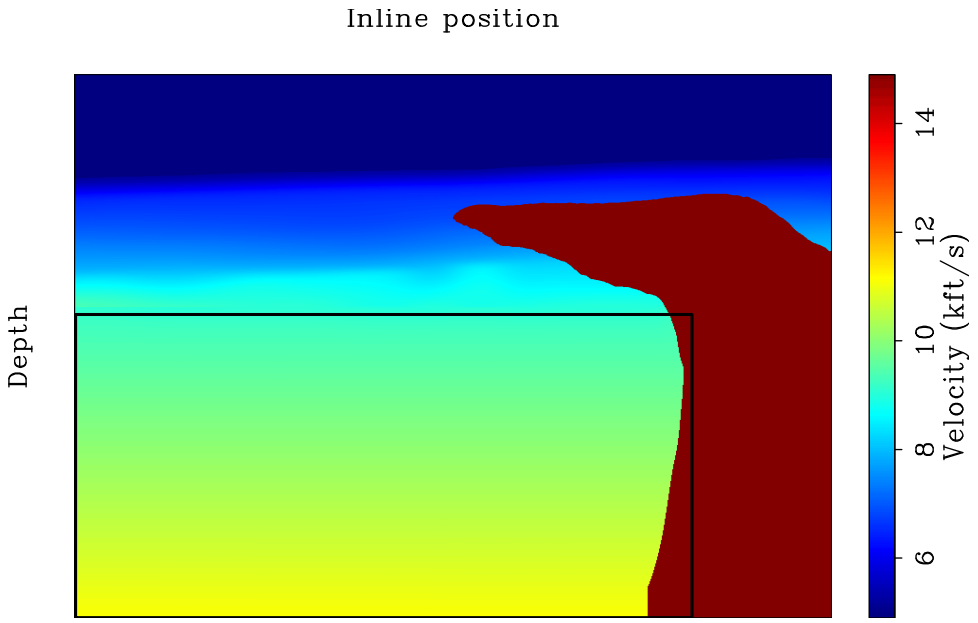

Figure 2: The initial velocity model for the selected 2-D line. The black box outlined area is the target region for velocity analysis. Velocities outside the region are assumed to be accurate. [**NR**]

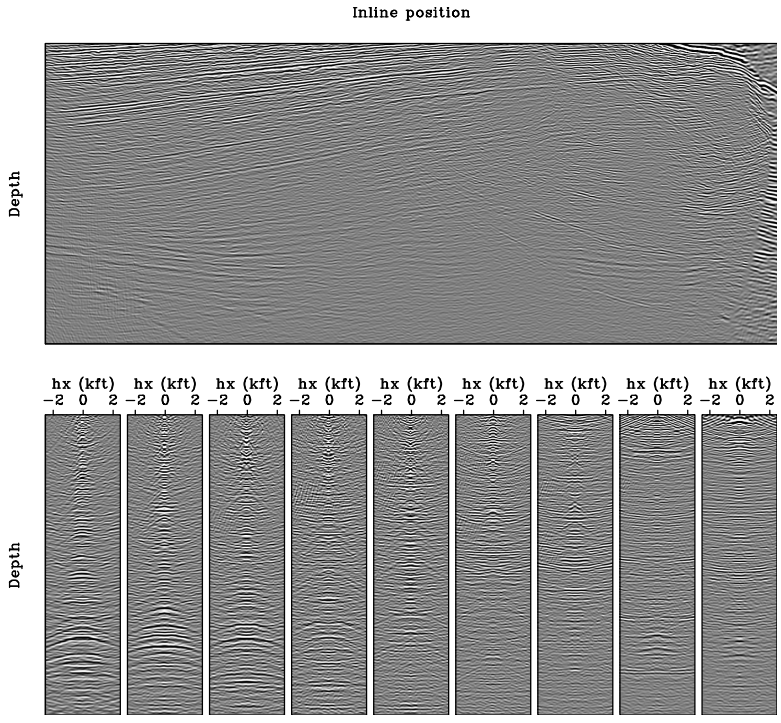

Figure 3: Initial target image and gathers obtained using the original data and the initial velocity shown in Figure 2. Top panel shows the stacked image (zero subsurface offset); bottom panel shows the SODCIGs for different horizontal locations. [**NR**]

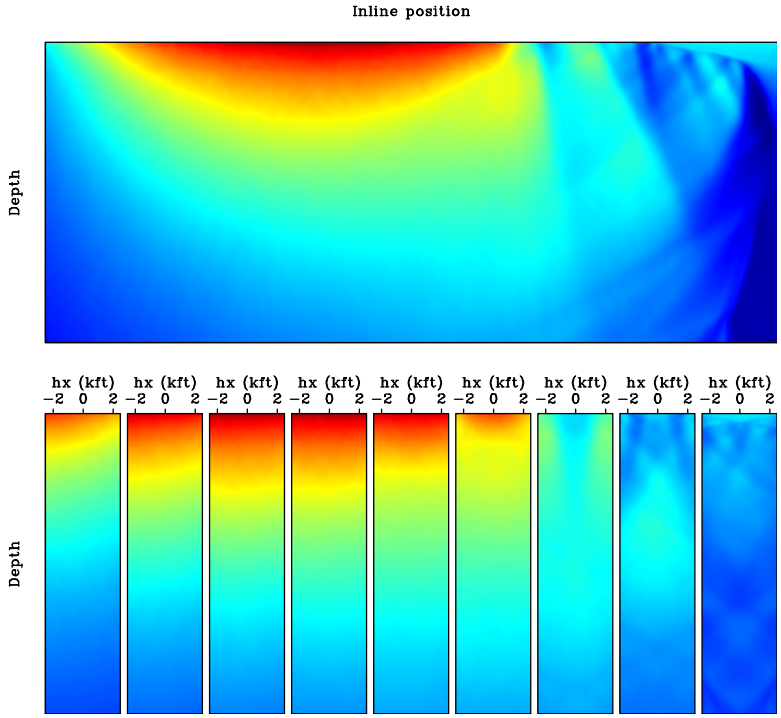

Figure 4: The diagonal of Hessian for the target region. View descriptions are the same as in Figure 3. [**NR**]

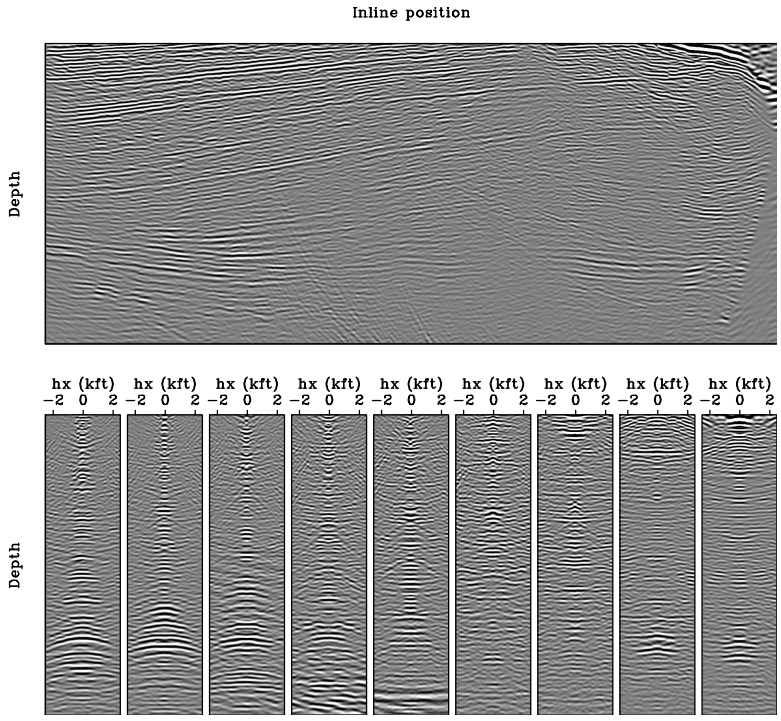

Figure 5: Image and gathers obtained using the new data set and the initial velocity (Figure 2). View descriptions are the same as in Figure 3. [**NR**]

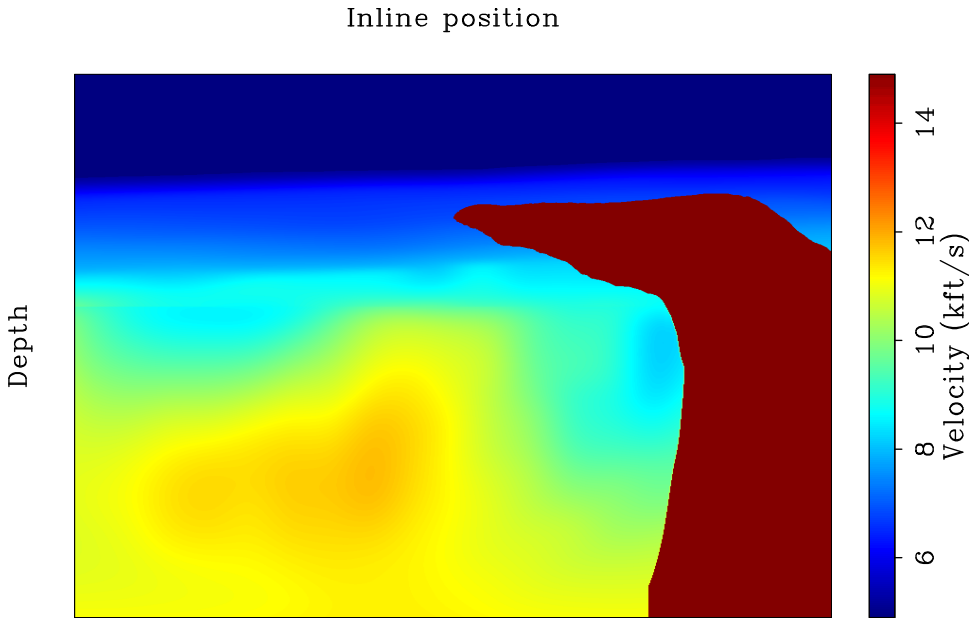

Figure 6: The inverted velocity model after 30 nonlinear iterations. [**NR**]

igrated Born data, which can be simulated in a target-oriented fashion and hence much smaller in size. Field-data examples demonstrate that the simulated new data set can successfully preserve velocity information that is useful for velocity analysis and can be used for velocity inversion with low computational cost.

ACKNOWLEDGMENTS

We thank BP and ExxonMobil for making the field data set available.

REFERENCES

Albertin, U., P. Sava, J. Etgen, and M. Maharramov, 2006, Adjoint wave-equation velocity analysis: SEG Technical Program Expanded Abstracts, **25**, 3345–3349.

Biondi, B., 2006, Prestack exploding-reflectors modeling for migration velocity analysis: SEG Technical Program Expanded Abstracts, **25**, 3056–3060.

———, 2007, Prestack modeling of image events for migration velocity analysis: **SEP-131**, 101–118.

Biondi, B., S. Fomel, and N. Chemingui, 1998, Azimuth moveout for 3-d prestack imaging: Geophysics, **63**, 574–588.

Biondi, B. and P. Sava, 1999, Wave-equation migration velocity analysis: SEG Technical Program Expanded Abstracts, **18**, 1723–1726.

Bleistein, N. and H. Jaramillo, H., 2000, A platform for Kirchhoff data mapping in scalar models of data acquisition: Geophysical Prospecting, **48**, 135–161.

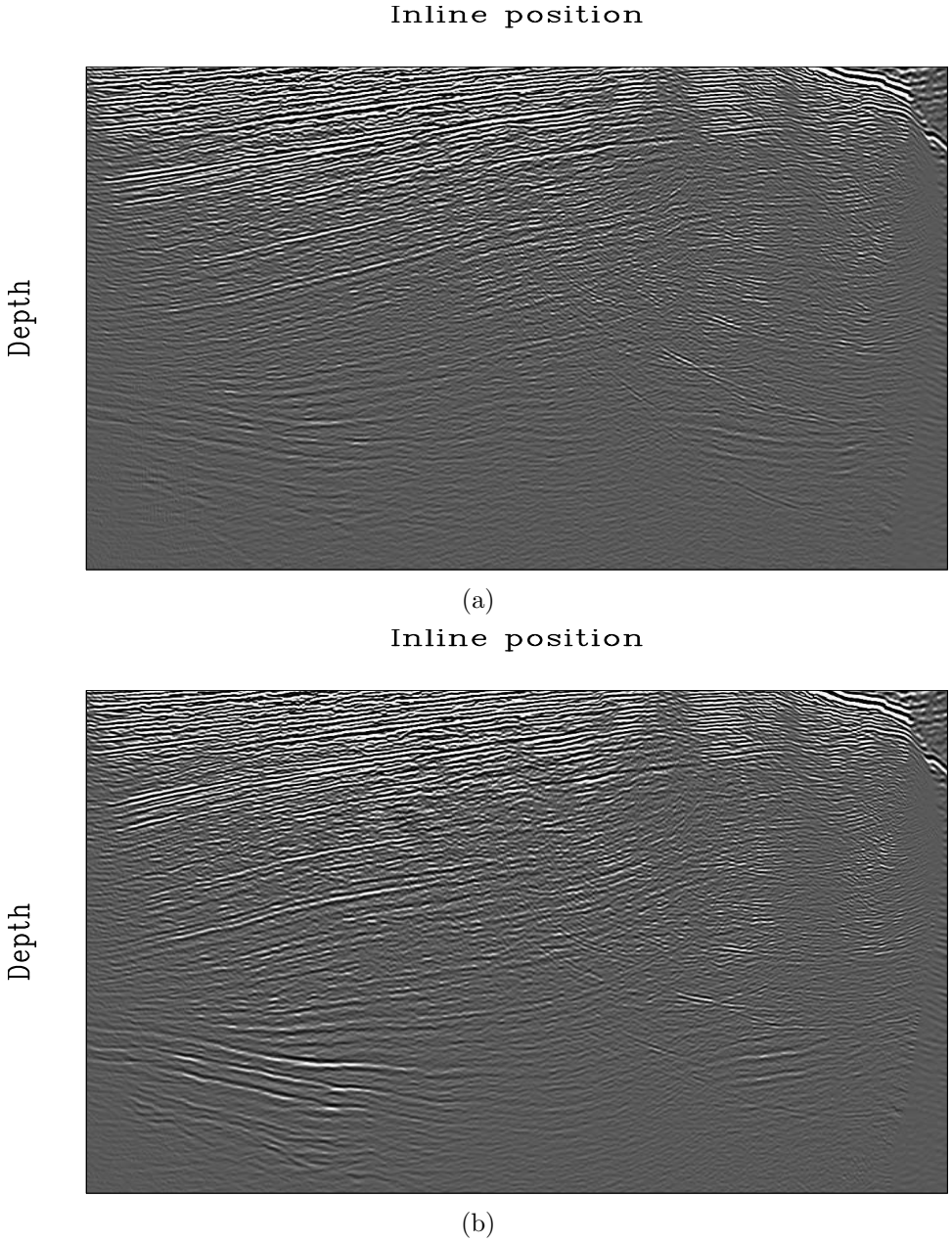

Figure 7: Stacked images (zero-subsurface-offset images) obtained using (a) the initial velocity model and (b) the inverted velocity model. The original data set is used for migration. [**NR**]

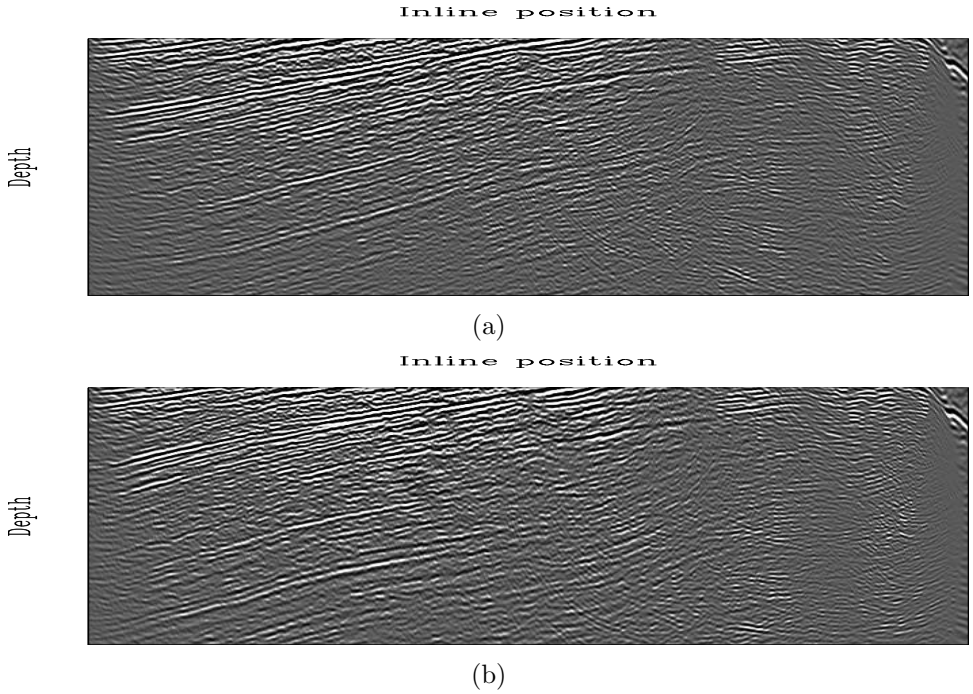

Figure 8: A close-up view of the upper section in Figure 7. (a) is obtained using the initial velocity model and (b) is obtained using the inverted velocity model. [**NR**]

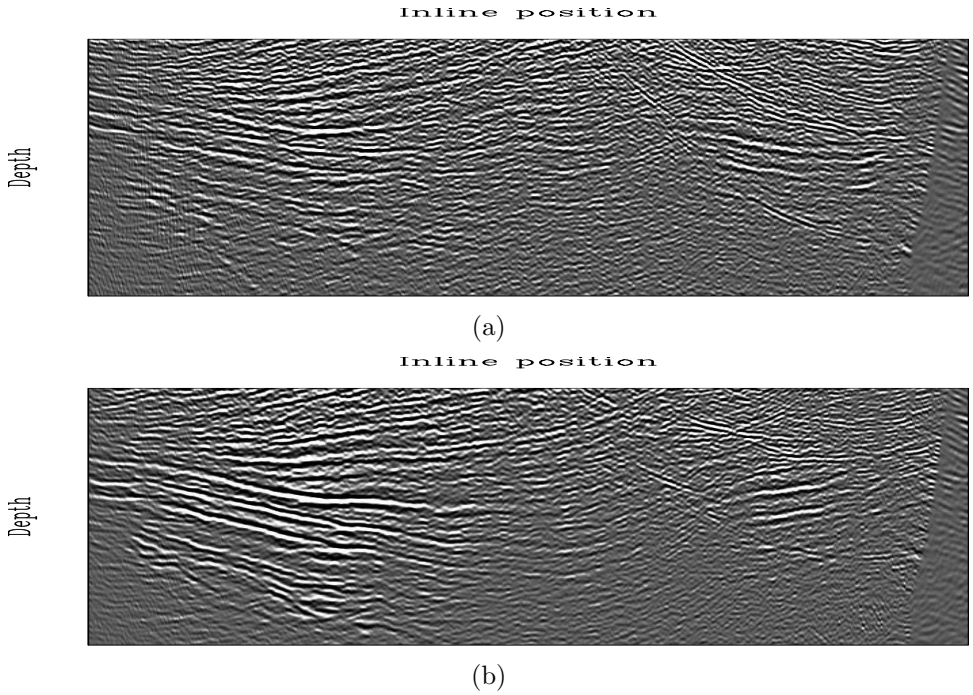

Figure 9: A close-up view of the lower section in Figure 7. (a) is obtained using the initial velocity model and (b) is obtained using the inverted velocity model. [**NR**]

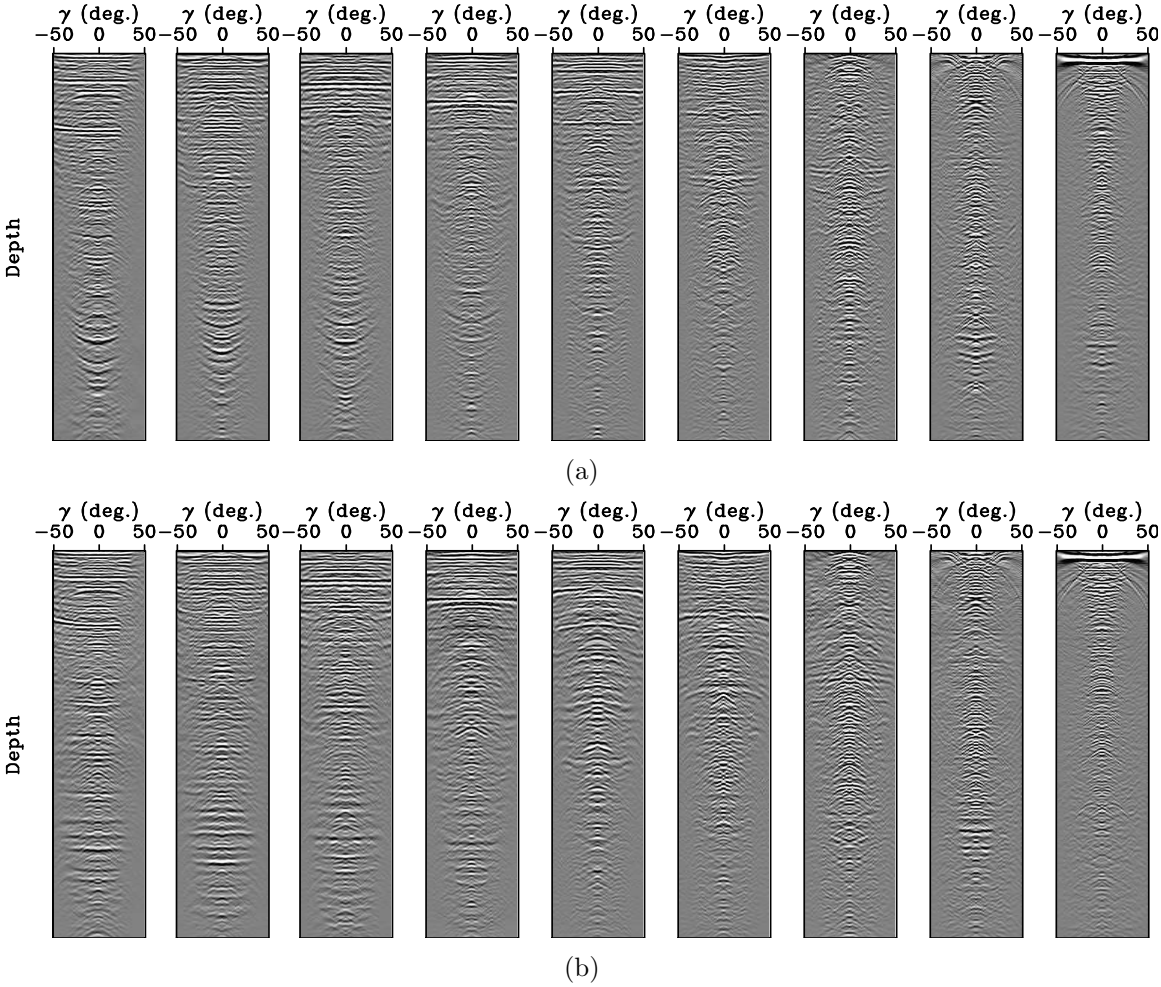

Figure 10: Angle-domain common-image gathers obtained using (a) the initial velocity model and (b) the inverted velocity model. The original data set is used for migration. [**NR**]

Guerra, C. and B. Biondi, 2010, Fast 3D velocity updates using the pre-stack exploding reflector model: **SEP-140**, 1–10.

Guerra, C., Y. Tang, and B. Biondi, 2009, Wave-equation tomography using image-space phase encoded data: SEG Technical Program Expanded Abstracts, **28**, 3964–3968.

Hoffmann, J., 2001, Illumination, resolution, and image quality of PP- and PS-waves for survey planning: The Leading Edge, **20**, 1008–1014.

Hubral, P., J. Schleicher, and M. Tygel, 1996, A unified approach to 3-D seismic reflection imaging, part I: Basic concepts: Geophysics, **61**, 742–758.

Mora, P., 1989, Inversion = migration + tomography: Geophysics, **54**, 1575–1586.

Plessix, R.-E. and W. A. Mulder, 2004, Frequency-domain finite-difference amplitude-preserving migration: Geophys. J. Int., **157**, 975–987.

Pratt, R. G., 1999, Seismic waveform inversion in the frequency domain, Part 1: Theory and verification in a physical scale model: Geophysics, **64**, 888–901.

Rickett, J. E., 2003, Illumination-based normalization for wave-equation depth migration: Geophysics, **68**, 1371–1379.

Sacchi, M. D. and T. J. Ulrych, 1995, High-resolution velocity gathers and offset space reconstruction: Geophysics, **60**, 1169–1177.

Sava, P., 2004, Migration and Velocity Analysis by Wavefield Extrapolation: PhD thesis, Stanford University.

Sava, P. and I. Vlad, 2008, Numeric implementation of wave-equation migration velocity analysis operators: Geophysics, **73**, VE145–VE159.

Shen, P., 2004, Wave-equation Migration Velocity Analysis by Differential Semblance Optimization: PhD thesis, Rice University.

Shen, P. and W. W. Symes, 2008, Automatic velocity analysis via shot profile migration: Geophysics, **73**, VE49–VE59.

Shen, P., W. W. Symes, S. Morton, A. Hess, and H. Calandra, 2005, Differential semblance velocity analysis via shot profile migration: SEG Technical Program Expanded Abstracts, **24**, 2249–2252.

Tang, Y., 2009, Target-oriented wave-equation least-squares migration/inversion with phase-encoded Hessian: Geophysics, **74**, WCA95–WCA107.

Tang, Y. and B. Biondi, 2010, Target-oriented wavefield tomography using demigrated Born data: **SEP-140**, 11–22.

Tang, Y., C. Guerra, and B. Biondi, 2008, Image-space wave-equation tomography in the generalized source domain: **SEP-136**, 1–22.

Tarantola, A., 1984, Inversion of seismic reflection data in the acoustic approximation: Geophysics, **49**, 1259–1266.

Trad, D. O., T. J. Ulrych, and M. D. Sacchi, 2002, Accurate interpolation with high-resolution time-variant radon transforms: Geophysics, **67**, 644–656.

Valenciano, A., 2008, Imaging by Wave-equation Inversion: PhD thesis, Stanford University.

Wang, B., F. Qin, F. Audebert, and V. Dirks, 2005, A fast and low cost alternative to subsalt wave equation migration perturbation scans: SEG Technical Program Expanded Abstracts, **24**, 2257–2260.

Woodward, M. J., 1992, Wave-equation tomography: Geophysics, **57**, 15–26.